ELSEVIER

Journal of Organometallic Chemistry 625 (2001) 173–179

Journal of Organometallic Chemistry

www.elsevier.nl/locate/jorganchem

Complexation behavior of 1,1″:1′,1‴-bis(1,4,10,13-tetraoxa-7,16-diazacyclooctadecane-7,16-diyldimethyl)bisferrocene: structural determination, NMR, ^{57}Fe Mössbauer and electrochemical measurements

Teng-Yuan Dong *[1], Liangshiu Lee *[2], Ching-Hung Cheng, Ling-Shao Chang, Michael Y. Chiang

Department of Chemistry, National Sun Yat-Sen University, Kaohsiung, Taiwan, ROC

Received 17 August 2000; received in revised form 5 October 2000; accepted 11 October 2000

Abstract

The complexing behavior of 1,1″:1′,1‴-bis(1,4,10,13-tetraoxa-7,16-diazacyclooctadecane-7,16-diyldimethyl)bisferrocene (**1**) toward KPF_6 ion was studied. To gain a better understanding into the factors which determine the extent of this redox-switched bonding in the complexation of KPF_6 by **1**, we carried out X-ray crystal structural determination, NMR, FAB-MS technique, cyclic voltammetry measurements, and ^{57}Fe Mössbauer analyses. We suggest that the KPF_6 salt of **1** is not a kinetically labile system. Our studies also provide direct evidence that ferrocene crown ether displays a drop in complex stability upon oxidation.

Keywords: Ferrocene; Cryptand; Metallocene; Mössbauer

1. Introduction

The ability of macrocycles to complex a variety of cations must be considered the key property of crown ethers and cryptands [1,2]. An early goal in crown and cryptand chemistry was to see if a macrocycle's inherent cation binding could be altered by a switching mechanism. Among the chemical subspecies that have been served as switches are pH switch, photochemical switch, thermal switch and oxidation–reduction switch.

Two classes of redox-switched crown ethers are known [3]. Anthraquinone-linked crown ethers [4] show increased bonding of cation upon reduction and ferrocene crown ethers [5,6] on the other hand display a sharp drop in complex stability upon oxidation. In the latter case, the key design principle is that ferrocene has a readily accessible redox couple such that neutral ferrocene can be converted easily into the ferrocenium cation. When the ferrocene unit is incorporated within the molecular framework of the crown ether, ferrocene's d-electrons may or may not serve as donors for a bound cation, but when the ferrocene unit is oxidized, a repulsive positive charge is placed in proximity to the bound cation. This chemical change diminishes the cation-binding capacity of the ligand which is switched from a high to a low binding state.

This paper reports the complexing behavior of 1,1″:1′,1‴-bis(1,4,10,13-tetraoxa-7,16-diazacyclooctadecane-7,16-diyldimethyl)bisferrocene (**1**) toward KPF_6 ion. To gain a better understanding into the factors which determine the extent of this redox-switched bonding in the complexation of KPF_6 by **1**, we carried out X-ray crystal structural determination. The crystal structure of the binuclear cryptate **1** formed with KPF_6 revealed that K^+ was encapsulated within the macrocyclic cavity, the same structure as recently reported by Plenio [7] for the bis-RbI adduct of **1** and by Hall [8] for the bis-$Ca(CF_3SO_3)_2$ adduct of **1**. This paper also reports the multinuclear NMR data, cyclic voltammetry measurements, and ^{57}Fe Mössbauer analyses.

[1] *Corresponding author. Fax: +886-7-5253908; e-mail: dty@mail.nsysu.edu.tw

[2] *Corresponding author. Fax: +886-7-5253908

0022-328X/01/$ - see front matter
PII: S0022-328X(00)00814-7

2. Results and discussion

A sample of 1,1″:1′,1‴-bis(1,4,10,13-tetraoxa-7,16-diazacyclooctadecane-7,16-diyldimethyl)bisferrocene was prepared simultaneously according to the literature procedure [6,9] by reaction of equimolar amounts of 1,1′-ferrocenedicarboxylic acid chloride with 4,13-diaza-18-crown-6 in the presence of Et_3N under high dilution conditions and then following reduction in THF with $LiAlH_4$. The KPF_6 complex of **1** was obtained by dissolving one equivalent of **1** in a solution containing two equivalents of the salt in CH_3OH–CH_3CN. The synthetic steps and the structure of the KPF_6 complex of **1** are shown in Scheme 1.

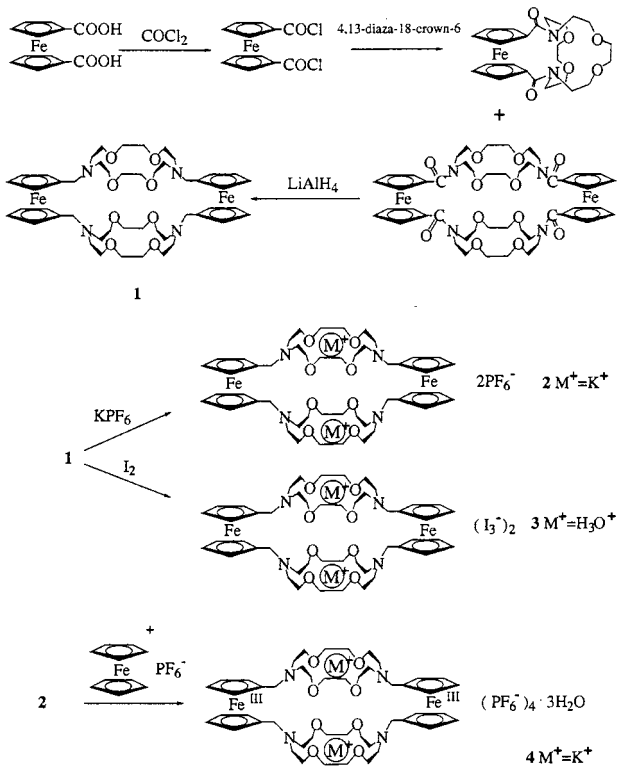

Scheme 1.

Table 1
Experimental and crystal data for the X-ray structure of **2**

Formula	$C_{48}H_{72}F_{12}Fe_2K_2N_4O_8P_2$
M_w	1312.94
Crystal system	Monoclinic
Space group	$P2_1/c$
a (Å)	11.553(4)
b (Å)	20.471(4)
c (Å)	12.860(4)
β (°)	106.36(3)
V (Å^3)	2918(1)
Z	2
D_{calc} (g cm^{-3})	1.494
μ (cm^{-1})	7.85
λ (Å)	0.71069
2θ limits (°)	50
Trans coefficient	0.9744–1.0000
R [a]	0.075
R_w [b]	0.067

[a] $R = \Sigma||F_o|-|F_c|| \Big/ \Sigma|F_o|$.

[b] $R_w = \left[\Sigma\, w(|F_o|-|F_c|)^2 \Big/ \Sigma(wF_0^2)\right]^{1/2}$.

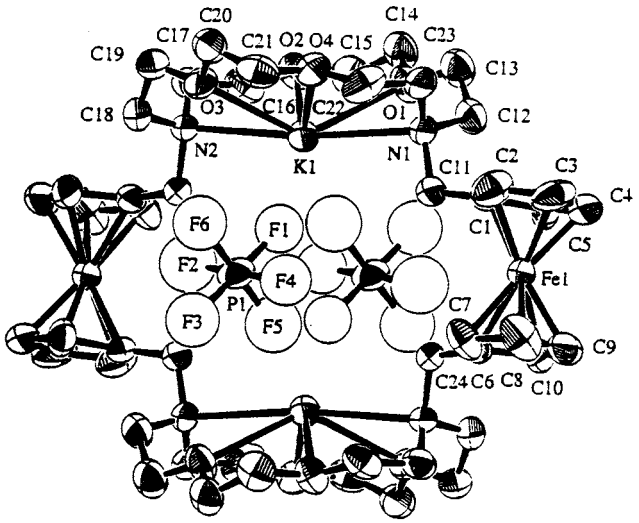

Fig. 1. Molecular view of **2**. Hydrogen atoms have been omitted for clarity.

2.1. Cation-binding studies

We chose single crystal X-ray determination, NMR, electrochemical measurements, and ^{57}Fe Mössbauer techniques to study the molecular structure and electronic situation when binding occurs.

2.1.1. Molecular structure of *1* binding K^+

Details of the X-ray crystal data collection and unit cell parameters are given in Table 1, and the molecular structure is shown in Fig. 1. Selected bond distances and angles are given in Table 2. Complete tables of positional parameters, bond distances, and bond angles are given as supplementary material.

In the crystal structure of **2** the molecule is situated on a crystallographic center of inversion. The bond lengths and angles about the Cp rings vary little and are close to those reported for analogous ferrocenes [10]. Inspection of the average bond distance between the Fe atom and the five carbons (Fe–C) and the average Fe–Cp distance for a ferrocenyl moiety shows that these values are also close to the corresponding value observed for ferrocene (2.045 Å for Fe–C and 1.65 Å for Fe–Cp) [10]. The two least-squares planes of the Cp rings for a given ferrocenyl moiety form a nearly parallel geometry with a tilting angle of 3.9°, while the two

Cp rings are also nearly eclipsed with an average staggered angle of 16(3)°.

When K^+ is bound, the macro-ring adjusts to what may be considered a binding conformation in which the four K^+–O distances are 2.838(6), 2.900(6), 2.842(6), and 2.885(6) Å and the average distance is 2.886(6) Å. In known K^+ complexes of crown ether, K^+–O are typically in the range 2.82 ± 0.07 Å [11].

Table 2
Selected bond distances and angles

Atoms involved	Angle (°) or distance (Å)
Fe–C [a]	2.028(10)
Fe–Cp [b]	1.638
C–C (Cp) [c]	1.41(1)
C–C (macro-ring) [d]	1.50(1)
C–N (macro-ring) [d]	1.46(1)
C–O (macro-ring) [d]	1.41(1)
K^+–N1	3.008(7)
K^+–N2	3.008(7)
K^+–O1	2.838(6)
K^+–O2	2.900(6)
K^+–O3	2.842(6)
K^+–O4	2.885(6)
K^+–F1	2.65(1)
K^+–F5	2.649(9)
Tilt angle [e]	3.9
Staggered angle [f]	16(3)

[a] The average bond distance between the Fe atom and the five carbons.

[b] The average distance between the Fe atom and the two least squares planes of Cp rings.

[c] The average C–C bond length in the Cp rings.

[d] The average C–C, C–N and C–O bond distances in the macro-ring.

[e] The dihedral angle between the least squares planes of the Cp rings.

[f] The average staggered angle for the two Cp rings.

Table 3
^{1}H- and ^{13}C- (δ values) NMR data of **2** in $CDCl_3$

^{13}C (ppm)	Assignment	^{1}H (integ., multi.)
	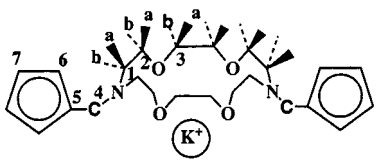	
49.93	C4	3.76 (8H, s)
51.22	C1	2.30 (8H, dd)
		2.60 (8H, dd)
67.68	C2, C7	3.37 (8H, dd)
		3.53 (8H, dd)
		4.10 (8H, dd)
70.39	C3	3.50 (8H, dd)
		3.73 (8H, dd)
70.44	C6	4.00 (8H, dd)
79.72	C5	

The PF_6^- anion is disordered about the F_5–P_1–F_6 vector. We assigned the major configuration to be 60% and the minor configuration to be 40%. In complex **2**, the non-equivalent P–F bond lengths in the PF_6^- anion suggest an electronic interaction between K^+ and PF_6^-. It is interesting to note that the K^+–F1 and K^+–F5 distance of 2.65(1) Å is even shorter than those of K^+–O and K^+–N bond lengths.

2.1.2. ^{1}H-NMR analysis of **2**

The KPF_6 binding bridged cryptand (**2**) has a complex ^{1}H-NMR spectrum. Furthermore, in the ^{1}H-NMR spectrum of **2** the uncomplexed species (**1**) is not observed. Assignments of the various protons could not be made on the basis of chemical shift alone but were established using ^{13}C–^{1}H heteronuclear (HQMC) and homonuclear (COSY) 2D NMR experiments. The chemical shifts and the assignments of all the protons and carbons are reported using the notation depicted in Table 3.

The ^{1}H-NMR spectrum of **2** shows two singlets for the ferrocene protons, two doublets of doublet protons for the hydrogens of the methylene groups α to nitrogen (on C1), two doublets of doublet patterns for the hydrogens of the $–CH_2–$ groups β to nitrogen (on C2), and two doublets of doublet for the hydrogens of the remaining glycolic linkages. The fact that the eight protons α to nitrogen, the eight protons β to nitrogen and 16 glycolic protons are each found as a pair of non-equivalent protons (a and b) provides strong evidence for a degree of rigidity within the cryptand moiety. It is quite interesting to note that in the case of **1**·2K(CF_3SO_3) the separated signals of protons 1a and 1b (protons α to nitrogen) were observed, but the separated signals of protons 2a and 2b (protons β to nitrogen) and the separated signals of protons 3a and 3b (glycolic protons) were unobserved [8]. The difference between **2** (i.e. **1**·2KPF_6) and **1**·2K(CF_3SO_3) is the counterion. Therefore, the difference in the ^{1}H-NMR results for **1**·2KPF_6 and **1**·2K(CF_3SO_3) can be ascribed to the existence of ion-pairing. We suggest that there is an electronic interaction between K^+ and PF_6^- in the solution state of **1**·2KPF_6.

2.1.3. ^{57}Fe Mössbauer spectral analysis

Several groups have used Mössbauer spectroscopy to investigate possible interaction of an encapsulated cation with a ferrocenyl macrocycle. In crown ether **5**, Akabori and coworkers reported [12] an increased quadrupole splitting (ΔE_Q) when a metal ion is complexed. They ascribed this to direct interaction between the metal cation and the iron atom. Hall and coworkers reported [13] that the values of isomer shift (IS) for the series of complexes **6** increase with increasing ionic radius of the group metal cations, although changes

Table 4
^{57}Fe Mössbauer data for **1** and **2** at 300 K

Compound	IS [a]	ΔE_Q [b]	Γ [c]
1	0.426	2.276	0.250, 0.250
2	0.426	2.276	0.261, 0.261
3	0.425	2.369	0.270, 0.290

[a] Isomer shift referenced to iron-foil in mm s^{-1}.
[b] Quadrupole-splitting in mm s^{-1}.
[c] Full width at half-height taken from the least-squares-fitting program. The width for the line at more positive velocity is listed first for each doublet.

Table 5
FAB mass spectral analysis of **2**

m/z	Relative intensity	Assignment [a]
1170	21.81	**1**($Fe^{II, II}$)+$2K^+$+PF_6+3H
1169	40.83	**1**($Fe^{II, II}$)+$2K^+$+PF_6+2H
1168	97.69	**1**($Fe^{II, II}$)+$2K^+$+PF_6+1H
985	44.74	**1**($Fe^{II, II}$)+K^++2H
984	7.98	**1**($Fe^{II, II}$)+K^++H
983	92.06	**1**($Fe^{II, II}$)+K^+
982	0.52	
981	25.59	
946	0.19	**1**($Fe^{II, III}$)+2H
945	0.44	**1**($Fe^{II, III}$)+H
944	0.76	**1**($Fe^{II, III}$)
584	18.78	**1**($Fe^{II, III}$)+$2K^+$+PF_6

[a] **1**($Fe^{n+, m+}$): molecular ion peak of **1** in which the oxidation states of the two Fe centers are in n^+ and m^+ states.

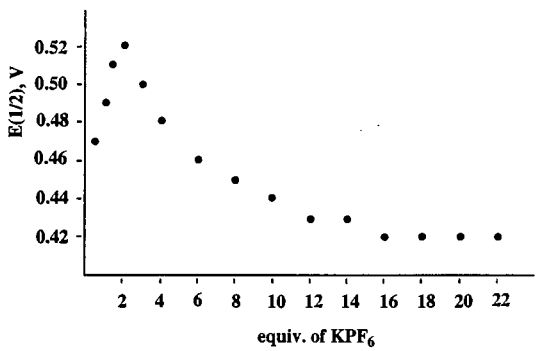

Fig. 2. Complexation-induced change in $E_{1/2}$ for the oxidation–reduction of **1** as a function of the equivalent of K^+ ion.

between individual complexes are small ($\pm$0.04 mm s^{-1}) (chart1.).

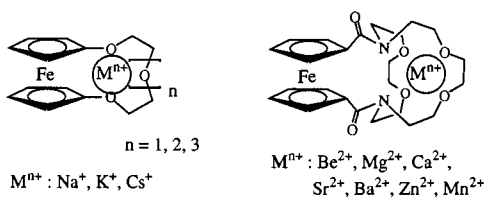

5 6

Chart 1.

The isomer shift and quadrupole splitting data for compounds **1** and **2** are given in Table 4. Uncomplexed and complexed samples gave a well-resolved quadrupole doublet in the Mössbauer spectrum, consistent with a distorted electronic structure around the ^{57}Fe nucleus. No variation in IS and ΔE_Q values between uncomplexed compound **1** and complexed compound **2** is observed. In other words, no direct interaction between the iron atom and K^+ ion is observed.

2.1.4. FAB-MS of compound 2

Fast atom bombardment mass spectrometry (FAB-MS) is a sensitive probe of solution phenomena and may be applied under a variety of conditions. Gokel and coworkers employed [6] this method to screen a variety of potential host molecules for their ability to bind cations. In FAB-MS technique, a ligand–cation complex formed in a solution matrix may be desorbed by a high energy atom beam. Thus, a broad survey has been accomplished in binding interactions in crown ethers and related systems. In general, the binding trends were assessed from the ratio of [macrocycle–cation] complex to protonated macrocycle.

In the present studies, a 10 kV Cs atom beam was used to desorb samples from the 3-nitrobenzyl alcohol FAB matrix. As noted in Table 5, significant ion intensities were observed for mass corresponding to the ions complexed with $2K^+$ and K^+. Indeed, the binding of $2K^+$ and K^+ is very similar. As is obvious from the data in the table, the ion intensities corresponding to the uncomplexed ion were significantly weaker than those of complexed ion. The bis(crown) diamine (**2**) has two macro-rings containing four basic amine groups and two ferrocenes that constitute a rigid box. This can afford one or two bound cations in a three-dimensional array. Gokel also employed [6] FAB-MS technique using an 8-kV xenon atom beam to assess the Na^+ binding interactions in bis(crown) diamine **1**. They found that the ratios of $[M^+ + Na^+]/[M^+ + H]$ and $[M^+ + 2Na^+]/[M^+ + 2H]$ are 45 and 8, M^+ used here as the molecular ion of **1**. Thus, the diamine **1** binds K^+ much more effectively than Na^+.

2.1.5. Cyclic voltammetry of 1 in the presence of K^+ ion

CV of a 1.0 mM solution of **1** in CH_2Cl_2:CH_3CN (1:1)–0.1 M (TBA)PF_6 yields a single set of waves centered at 0.46 V versus a Ag | AgCl electrode at 25°C that corresponds to the reversible oxidation of the ferrocene moiety. As shown in Fig. 2, addition of various concentrations of KPF_6 to the same solution shifts the observed half-wave potentials; that is, the potential of redox couple shifts gradually as the concentration of the interacting additive (KPF_6) increases until a maximum value of 0.52 V is reached at two equiva-

lents of KPF_6. This latter value is ascribed to the half-wave potential of the corresponding complex species. This also reveals strong binding of **1** with $2K^+$ in CH_2Cl_2–CH_3CN solution.

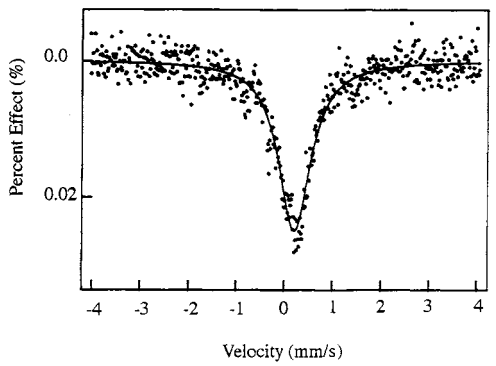

Fig. 3. ^{57}Fe Mössbauer spectrum of **4** at 300 K.

Table 6
FAB mass spectral analysis of **4**

m/z	Relative intensity	Assignment [a]
1316	3.37	**1**($Fe^{II, III}$)+$2K^+$+$2PF_6$+4H
1315	11.20	**1**($Fe^{II, III}$)+$2K^+$+$2PF_6$+3H
1314	13.31	**1**($Fe^{II, III}$)+$2K^+$+$2PF_6$+2H
1313	24.68	**1**($Fe^{II, III}$)+$2K^+$+$2PF_6$+H
1312	1.50	**1**($Fe^{II, III}$)+$2K^+$+$2PF_6$
1311	3.94	**1**($Fe^{II, III}$)+$2K^+$+$2PF_6$
1278	19.56	**1**($Fe^{III, III}$)+K^++$2PF_6$+5H
1277	31.17	**1**($Fe^{III, III}$)+K^++$2PF_6$+4H
1276	67.53	**1**($Fe^{III, III}$)+K^++$2PF_6$+3H
1275	11.85	**1**($Fe^{III, III}$)+K^++$2PF_6$+2H
1274	8.28	**1**($Fe^{III, III}$)+K^++$2PF_6$+H
1273	0.91	**1**($Fe^{III, III}$)+K^++$2PF_6$
1272	2.01	**1**($Fe^{III, III}$)+K^++$2PF_6$
1171	7.39	**1**($Fe^{II, II}$)+$2K^+$+PF_6+4H
1170	12.26	**1**($Fe^{II, II}$)+$2K^+$+PF_6+3H
1169	23.70	**1**($Fe^{II, II}$)+$2K^+$+PF_6+2H
1168	35.39	**1**($Fe^{II, II}$)+$2K^+$+PF_6+H
1167	3.79	**1**($Fe^{II, II}$)+$2K^+$+PF_6
1166	4.75	**1**($Fe^{II, II}$)+$2K^+$+PF_6
1132	11.04	**1**($Fe^{II, III}$)+K^++PF_6+4H
1131	16.31	**1**($Fe^{II, III}$)+K^++PF_6+3H
1130	40.58	**1**($Fe^{II, III}$)+K^++PF_6+2H
1129	5.36	**1**($Fe^{II, III}$)+K^++PF_6+H
1128	6.25	**1**($Fe^{II, III}$)+K^++PF_6
987	3.65	**1**($Fe^{II, II}$)+K^++4H
986	13.80	**1**($Fe^{II, II}$)+K^++3H
985	31.17	**1**($Fe^{II, II}$)+K^++2H
984	59.09	**1**($Fe^{II, II}$)+K^++H
983	9.58	**1**($Fe^{II, II}$)+K^+
982	12.91	**1**($Fe^{II, II}$)+K^+
946	3.21	**1**($Fe^{II, III}$)+2H
945	3.98	**1**($Fe^{II, III}$)+H
944	4.69	**1**($Fe^{II, III}$)
943	2.62	**1**($Fe^{II, III}$)
658 [b]	0.82	**1**($Fe^{III, III}$)+2K++2PF6+2H
657	4.12	**1**($Fe^{III, III}$)+$2K^+$+$2PF_6$+H
656	8.12	**1**($Fe^{III, III}$)+$2K^+$+$2PF_6$

[a] **1**($Fe^{n+, m+}$): molecular ion peak of **1** in which the oxidation states of the two Fe centers are in n^+ and m^+ states.
[b] Dication.

2.2. Oxidation reaction of *1* with I_2

Ferrocenium triiodide can be easily prepared by oxidizing the corresponding neutral ferrocene with I_2 [14]. The reaction product of **1** with I_2 is not a typical ferrocenium triiodide salt. Compound **3** was obtained by adding a benzene–hexane (1:1) solution containing a stoichiometric amount of I_2 to a benzene–hexane (1:1) solution of **1**. The resulting red–brown triiodide salt (**3**) is not an expected ferrocenium compound. The Fe(II) oxidation state is concluded from the ^{57}Fe Mössbauer technique. The ferrocenyl group gives a spectrum characterized by a large quadrupole splitting in the range 2.0–2.5 mm s^{-1}, while the spectrum of ferrocenium cation is characterized by small or vanishing quadrupole splitting [14]. The ^{57}Fe Mössbauer spectrum of **3** was obtained at 300 K. The absorption peaks were fitted to Lorentzian lines, and the resulting fitting parameters are summarized in Table 4. Compound **3** gives a single doublet, which is expected for an Fe(II) metallocene. Thus, the triiodide anion is a counterion for macrocycle bound H_3O^+ molecular cation.

2.3. Oxidation reaction of *2* with ferrocenium PF_6

Compound **2** can be easily oxidized by ferrocenium PF_6 as oxidizing agent. As shown in Scheme 1, compound **4** was obtained by mixing a stoichiometric amount of **2** and ferrocenium PF_6 in CH_2Cl_2 at 0°C. The resulting dark green product is an expected ferrocenium compound characterized by ^{57}Fe Mössbauer technique. The ^{57}Fe Mössbauer spectrum of **4** was obtained at 300 K. As shown in Fig. 3, compound **4** gives an absorption peak with vanishing quadrupole splitting, which is expected for an Fe(III) metallocene.

2.4. Cation binding studies of *4* by FAB-MS

Bisferrocenium compound **4** is of use in understanding the influence of ferrocenium moieties on the binding capacity of the crown ether ligand. It has been suggested [6] that ferrocene crown ethers display a sharp drop in the binding capacity upon oxidation. Therefore, it is of interest to see whether the ferrocenium moieties in **4** and its instantaneous repulsive positive charge affect the binding capacity and the complex stability.

As noted in Table 6, significant ion intensities were observed for mass corresponding to the ferrocenium or ferrocenyl crown ether ions complexed with $2K^+$ ion or K^+ ion. The mass at m/z 1313 is assigned to the ion **1**($Fe^{II, III}$) + $2K^+$ + $2PF_6$ + H, where **1**($Fe^{II, III}$) denotes the molecular framework of **1** in which the oxidation states of the two Fe centers are in II and III states. The

mass at m/z 1168 is assigned to $\mathbf{1}(Fe^{II,\ II}) + 2K^+ + PF_6 + H$ and the dication peak at m/z 657 is assigned to $\mathbf{1}(Fe^{III,\ III}) + 2K^+ + 2PF_6 + H$. Making a comparison of the relative intensities for these three peaks, we can conclude that the binding capacity with $2K^+$ decreases as the ferrocenyl moiety is oxidized to ferrocenium ion. Similarly, from a comparison of the relative intensities at m/z 1274, 1129 and 984, we also conclude that the trend of binding capacity with $1K^+$ ion is $\mathbf{1}(Fe^{II,\ II}) > \mathbf{1}(Fe^{II,\ III}) \cong \mathbf{1}(Fe^{III,\ III})$.

3. Conclusions

The K^+ complexation behavior of **1** was studied by X-ray structural determination, NMR, FAB-MS technique, and electrochemical measurements. Indeed, these studies conclude compound **2** is not a kinetically labile system. ^{57}Fe Mössbauer measurement of **2** also confirm that there is no interaction between K^+ and Fe(II) center. Our studies also provide direct evidence that ferrocene crown ether displays a drop in complex stability upon oxidation.

4. Experimental

4.1. General information

All manipulations involving air-sensitive materials were carried out using standard Schlenk techniques under an atmosphere of N_2. Chromatography was performed on neutral alumina (Merck, activity II). Solvents were dried as follows: benzene, ether, and tetrahydrofurane were distilled from Na–benzophenone; dichloromethane was distilled from CaH_2; *N*,*N*,*N*′,*N*′-tetramethylethylenediamine was distilled from KOH.

4.2. Ferrocene starting materials

Samples of 1,1′-dibromoferrocene [15], 1,1′-ferrocenedicarboxylic acid [6], 1,1′-ferrocenedicarboxylic acid chloride [16], and ferrocenium PF_6 [17] were prepared according to the literature procedure.

4.3. 1,1″:1′,1‴-Bis(1,4,10,13-tetraoxa-7,16-diazacyclooctadecane-7,16-diyldimethyl)-bisferrocene (1)

Compound **1** was prepared according to the literature procedure by reaction of equimolar amounts of 1,1′-ferrocenedicarboxylic acid chloride and 4,13-diaza-18-crown-6 in the presence of Et_3N with benzene as the solvent under high dilution conditions (7 mM), and then followed the reduction reaction with $LiAlH_4$ [6].

4.4. K^+ complexation of 1

The KPF_6 complex of **1** was obtained by dissolving 0.1 g (0.164 mmol) of **1** in a solution containing 0.061 g (0.164 mmol) of the KPF_6 salt in methanol (20 ml) and CH_3CN (10 ml). The mixture was allowed to reflux for 10 h. The solvent was evaporated under reduced pressure to afford an orange solid. The product was recrystallized from CH_2Cl_2–hexane (0.12 g, 55%). Anal. Calc. for $C_{48}H_{72}F_{12}Fe_2K_2N_4O_8P_2$: C, 43.91; H, 5.53; N, 4.27. Found: C, 43.65; H, 5.52; N, 4.22%.

4.5. Reaction of 1 with I_2 (3)

A sample of **3** was prepared by adding a benzene/hexane (1:1) containing three equivalents I_2 to a benzene–hexane (1:1) solution of **1** at 0°C. The resulting red–brown crystals were filtered and washed repeatedly with cold hexane. Recrystallization can be carried out from CH_2Cl_2–hexane. Anal. Calc. for **3** ($C_{48}H_{80}Fe_2I_6N_4O_{11}$): C, 33.05; H, 4.51; N, 3.21. Found: C, 33.53; H, 4.49; N, 3.10%.

4.6. Reaction of 2 with ferrocenium PF_6

A sample of **4** was prepared by stirring a mixture of two equivalents of ferrocenium PF_6 and one equivalent of **1** in CH_2Cl_2 for 2 h. To the reaction mixture was added a solution of hexane to precipitate a dark-green solid. The product was recrystallized from a CH_2Cl_2–hexane solution. Anal. Calc. for **4** ($C_{48}H_{78}F_{24}Fe_2K_2N_4O_{11}P_4$): C, 34.80; H, 4.75; N, 3.38. Found: C, 34.53; H, 4.46; N, 3.52%.

4.7. Physical methods

^{57}Fe Mössbauer measurements were made on a constant-velocity instrument which has been previously described. The absolute temperature accuracy is estimated to be ± 5 K, while the relative precision is ± 0.5 K. Computer fitting of the ^{57}Fe Mössbauer data to Lorentzian lines was carried out with a modified version of a previously reported program [18]. Velocity calibrations were made using a 99.99% pure 10-μm iron foil. Typical line widths for all three pairs of iron foil lines fell in the range 0.24–0.27 mm s^{-1}. Isomer shifts are reported relative to iron foil at 300 K but are uncorrected for temperature-dependent, second-order Doppler effects. It should be noted that the isomer shifts illustrated in the figures are plotted as experimentally obtained. Tabulated data are provided.

^{1}H-NMR spectra were run on a Varian INOVA-500 MHz spectrometer.

Electrochemical measurements were carried out with a BAS 100W system. Cyclic voltammetry was performed with a stationary glassy carbon working elec-

trode, which was cleaned after each run. These experiments were carried out with 1×10^{-3} M solution of bisferrocene in dry CH_2Cl_2–CH_3CN (1:1) containing 0.1 M of $(n\text{-}C_4H_9)_4NPF_6$ as supporting electrolyte. The potentials quoted in this work are relative to a Ag | AgCl electrode at 25°C. Under these conditions, ferrocene shows a reversible one-electron oxidation wave ($E_{1/2} = 0.46$ V).

Mass spectra were obtained with a VG-BLOTECH-QUATTRO 5022 system. A 10-kV Cs atom beam was used to desorb the sample from the 3-nitrobenzylalcohol FAB matrix. Binding trends were assessed from the ratio of [macrocycle–cation] complex to protonated macrocycle.

4.8. Structural determination of **2**

A red–brown crystal ($0.41 \times 0.43 \times 0.54$ mm) was grown when a layer of hexane was allowed to slowly diffuse into a CH_2Cl_2 solution of **2**. Data were collected on a Rigaku AFC7S diffractometer with graphite monochromated Mo–K_α radiation. Cell dimensions were obtained from 25 reflections with $10.69 < 2\theta < 14.87°$. The $\omega - 2\theta$ scan technique was used to record the intensities for all reflections for which $2\theta < 50°$. Of the 5308 unique reflections, there were 3029 reflections with $F_o > 3.0\sigma(F_o^2)$, where $\sigma(F_o^2)$ were estimated from counting statistics.

The structure was solved by direct methods and expanded using Fourier techniques. Non-hydrogen atoms were refined anisotropically. Hydrogen atoms were calculated with ideal geometries ($d_{C-H} =$ 0.95 Å). The X-ray crystal data are summarized in Table 1.

5. Supplementary material

Tables listing the final positional parameters for all atoms, the complete tables of bond distances and angles, and thermal parameters are available upon request from the author. Crystallographic data for the structural analysis have been deposited with Cambridge Crystallographic Data Centre, CCDC no. 150284 for compound **2**. Copies of this information may be obtained free of charge from The Director, CCDC, 12 Union Road, Cambridge CB2 1EZ, UK (Fax: +44-1223-336033; e-mail: deposit@ccdc.cam.ac.uk or www: http://www.ccdc.cam.ac.uk).

Acknowledgements

Acknowledgements are made to the National Science Council (NSC89-2113-M-110-003), Taiwan, ROC, and Department of Chemistry at Sun Yat-Sen University.

References

[1] (a) G.W. Gokel, Crown Ethers and Cryptands; Royal Society of Chemistry, London, 1991. (b) A.E. Kaifer, L.A. Echegoyen, in: Y. Inoue, G.W. Gokel (Eds.), Cation Binding by Macrocyclic Systems, Marcel Dekker, New York, 1990, p. 363. (c) E. Weber, J.L. Toner, I. Goldberg, F. Vögtle, D.A. Laidler, J.F. Stoddart, R.A. Bartsch, C.L. Liotta, in: S. Patai, Z. Rappoport (Eds.), Crown Ethers and Analogs, Wiley, New York, 1989. (d) C.D. Hall, in: A. Togni, T. Hayashi (Eds.), Ferrocenes, VCH, Weinheim, 1995, p. 280.
[2] (a) J.-M. Lehn, Acc. Chem. Res. 11 (1978) 49. (b) G. Runghino, S. Romano, J.-M. Lehn, G. Wipff, J. Am. Chem. Soc. 107 (1985) 7873. (c) J.M. Lehn, Angew. Chem. Int. Ed. Engl. 27 (1988) 89.
[3] (a) P.D. Beer, Adv. Inorg. Chem. 39 (1992) 79. (b) P.D. Beer, J.P. Danks, D. Hesek, J.F. McAleer, J. Chem. Soc. Chem. Commun. (1993) 2107. (c) P.D. Beer, D.B. Crowe, M.I. Ogden, M.G.B. Drew, B. Main, J. Chem. Soc. Dalton Trans. (1993) 2107. (d) N.D. Lowe, C.D. Garner, J. Chem. Soc. Dalton Trans. (1993) 3333. (e) C.D. Hall, J.H.R. Tucker, S.Y.F. Chu, A.W. Parkins, S.C. Nyborg, J. Chem. Soc. Chem. Commun. (1993) 1505.
[4] (a) L. Echegoyen, Y. Hafez, R.C. Lawson, J. de Mendoza, T. Torres, J. Org. Chem. 58 (1993) 2009. (b) S.R. Miller, D.A. Gustowski, Z. Chen, G.W. Gokel, L. Echegoyen, A.E. Kaifer, Anal. Chem. 60 (1988) 2021.
[5] W.E. Geiger, in: W.C. Trogler (Ed.), Organometallic Radical Process, Elsevier, Amsterdam, 1990, p. 142.
[6] J.C. Medina, T.T. Goodnow, M.T. Rojas, J.L. Atwood, B.C. Lynn, A.E. Kaifer, G.W. Gokel, J. Am. Chem. Soc. 114 (1992) 10583.
[7] H. Plenio, R. Diodone, J. Organomet. Chem. 492 (1995) 73.
[8] C.D. Hall, A. Leineweber, J.H.R. Tucker, D.J. Williams, J. Organomet. Chem. 523 (1996) 13.
[9] P.J. Hammond, A.P. Bell, C.D. Hall, J. Chem. Soc. Perkin Trans. 1 (1983) 707.
[10] P. Seiler, J.D. Dunitz, Acta Crystallogr. Sect. B 35 (1979) 1068.
[11] (a) D.T. Rosa, D. Coucouvanis, Inorg. Chem. 37 (1998) 2328. (b) P. Dapporto, P. Paoli, I. Matijai, L. Tuek-Boi, Inorg. Chim. Acta 252 (1996) 383.
[12] (a) S. Akabori, S. Shibahara, Y. Habata, M. Sato, Bull. Chem. Soc. Jpn. 57 (1984) 63. (b) S. Akabori, Y. Habata, Y. Sakamoto, M. Sato, S. Ebine, Bull. Chem. Soc. Jpn. 56 (1983) 537.
[13] C.D. Hall, I.P. Danks, P.J. Hammond, N.W. Sharpe, M.J.K. Thomas, J. Organomet. Chem. 388 (1990) 301.
[14] (a) T.-Y. Dong, D.N. Hendrickson, K. Iwai, M.J. Cohn, A.L. Rheingold, H. Sano, S. Motoyama, J. Am. Chem. Soc. 107 (1985) 7996. (b) T.-Y. Dong, C.H. Huang, C.K. Chang, Y.S. Wen, S.L. Lee, J.A. Chen, W.Y. Yeh, A. Yeh, J. Am. Chem. Soc. 115 (1993) 6357.
[15] R.F. Kovar, M.D. Rausch, H. Rosenberg, Organomet. Chem. Syn. 1 (1971) 173.
[16] P. Petrovitch, Double Liaison 133 (1966) 1093; Chem. Abstr. 68 (1968) 29843g.
[17] D.N. Hendrickson, Y.S. Sohn, H.B. Gray, Inorg. Chem. 10 (1971) 1559.
[18] J.F. Lee, M.D. Lee, P.K. Tseng, Chemistry 45 (1987) 50.